In-situ observations of supercooled liquid clouds over the Southern Ocean during the HIAPER Pole-to-Pole Observation (HIPPO) campaigns

Thomas H. Chubb,[1] Jorgen B. Jensen,[2] Steven T. Siems,[1] Michael J. Manton[1]

Corresponding author: Thomas H. Chubb, School of Mathematical Sciences, P.O. Box 28 M, Monash University, VIC 3800, Australia. (thomas.chubb@monash.edu)

[1]School of Mathematical Sciences, Monash University, Melbourne, Victoria, Australia

[2]Research Aviation Facility, NCAR Earth Observing Laboratory, Broomfield, Colorado, USA

Clouds over the Southern Ocean exist in a pristine environment that results in unique microphysical properties. However, in-situ observations of these clouds are rare, and the dominant precipitation processes are unknown. Uncertainties in their life cycles and radiative properties make them interesting from a weather and climate perspective. Data from the standard cloud physics payload during the HIAPER Pole-to-Pole Observations (HIPPO) global transects provide a unique snapshot the nature of low-level clouds in the Southern Ocean. High quantities of supercooled liquid water (up to $0.47\,\mathrm{g\,m^{-3}}$) were observed in clouds as cold as -22° C during two flights in different seasons and different meteorological conditions, supporting climatologies inferred from satellite observations. Cloud droplet concentrations were calculated from mean droplet size and liquid water concentrations, and were in the range of 30–$120\,\mathrm{cm^{-3}}$, which is fairly typical for the pristine Southern Ocean environment. Ice in non- or lightly-precipitating clouds was found to be rare, while drizzle drops with diameter greater than $100\,\mu$m formed through warm rain processes were widespread. Large, pristine crystals were commonly seen in very low concentrations below cloud base.

1. Introduction

The presence of "supercooled" liquid water (SLW; where liquid droplets exist at $T < 0^\circ$ C) in clouds is important to the understanding of both the radiative budget, due to enhanced short wave scattering compared to ice clouds [*Greenwald et al.*, 1995], and in the development of precipitation. Supercooled clouds are also an aviation hazard due to their role in airframe icing [*Politovich*, 1989].

Pure water droplets in laboratory settings can exist at temperatures as low as −38 to -40° C, before freezing occurs. In the real-world SLW exists in a metastable equilibrium in which the presence of ice nucleating particles (IN) can initiate droplet freezing at temperatures much warmer than this. The physical and chemical nature of the IN affects the freezing temperature, and accordingly, temperature-only parameterizations of cloud ice nucleation (as commonly used in numerical simulations) have been shown to be insufficient. *DeMott et al.* [2010] showed that typical temperature-only parameterisations of cloud ice nucleation resulted in radiative forcing discrepancies on the order of 1 $\mathrm{W\,m^{-2}}$ compared to better-constrained estimates.

Particles that nucleate ice at temperatures warmer than about −15 C are rare, consisting of one in 10^3 to one in 10^5 [*Rogers et al.*, 1998]. In the remote Southern Ocean (SO) this translates to concentrations as low as $0.01\,\mathrm{L^{-1}}$ [*Bigg*, 1973]. IN are generally assumed to be of mineral (i.e. dust) origin, but there are very few sources of dust for the SO. Biogenic particles of oceanic origin are presumed to be IN sources for the SO [*Burrows et al.*, 2013], but the link is generally inferred from temporal or spatial correlations, rather than of direct evidence of biological particles acting as IN.

Satellite-based lidar observations of SLW are especially common over the SO [*Hu et al.*, 2010], with SLW observed in 80% of clouds with temperature between 0 and −40° C. Spectroradiometer SLW retrievals occur in both summer (DJF) and winter (JJA) with absolute frequencies (i.e. of all pixels) above 30% at 50° S [*Morrison et al.*, 2011]. The synergy of the "A-Train" [*Stephens et al.*, 2002] satellites can be used to enhance the representation of cloud characteristics. *Huang et al.* [2012] used a merged radar/lidar/spectroradiometer cloud product [*Delanoë and Hogan*, 2010] to perform a cloud climatology, highlighting the extensive presence of supercooled liquid clouds over the SO, particularly during summer. However, satellite retrievals of SLW presence and quantity have remained unverified by in-situ observations over the SO.

There is mounting evidence that SO clouds are poorly simulated in both reanalysis and coupled global climate models, with the widespread biases in top-of-atmosphere radiation occurring in this region. *Trenberth and Fasullo* [2010] analyzed output from the Coupled Model Inter-comparison Project and showed that while biases in outgoing long wave and absorbed solar radiation (ASR) were compensatory, over the SO (45° – 65° S) there was a large discrepancy in the radiation budget due to excess ASR.

Elsewhere there have been a number of aircraft studies examining SLW in clouds. *Rauber and Tokay* [1991] attributed frequent observations of thin SLW layers at the top of clouds to an imbalance in the condensate supply rate and ice crystal growth rates. *Hobbs and Rangno* [1998] identified liquid-topped clouds precipitating ice to temperatures as low as −31°C as the dominant mixed-phase cloud structure in the Beaufort Sea, while *Rangno and Hobbs* [2001] found high ice particle concentrations in slightly to moderately supercooled Arctic stratocumulus cloud, identifying secondary ice mechanisms (crystal fragmentation/freezing droplet shattering) as likely causes. *Korolev et al.* [2003] examined 44000 km of in-cloud flight legs from the Arctic and continental North America, finding that all of the cloud sampled tended to be dominated by either liquid or ice, and for temperatures warmer than $-25°$ C a substantial fraction of the clouds were predominantly liquid.

The "warm rain" process, or droplet growth through collision and coalescence, can also occur in supercooled clouds. Also termed "freezing drizzle", the supercooled warm rain processes (SWRP) has been the subject of a number studies. *Rasmussen et al.* [2002] reproduced freezing drizzle conditions using bin microphysics in the MM5 model for a number of different observational studies, finding that both cloud condensation nuclei (CCN) concentrations and ice crystal concentrations played an important role in the growth of large droplets. *Rosenfeld et al.* [2013] observed supercooled rain and drizzle in pristine conditions in Alaska and northern California, finding extremely low concentrations ($0.03\,L^{-1}$) of ice crystals in layer clouds in spite of temperatures as low as $-21°$ C. In a similar environment (the Oregon Cascades), *Ikeda et al.* [2007] observed supercooled drizzle at temperatures as low as -19 C.

With the primary objective of conducting a global survey of climatically important aerosols and trace gases, the NSF/NCAR HIAPER (a high-performance research aircraft based on a Gulfstream V jet), conducted five global transects in different seasons between 2009 and 2011 for the HIAPER Pole-to-Pole Observation (HIPPO) campaign [*Wofsy and HIPPO Science Team*, 2011].Basic cloud microphysics instruments were operated in addition to the primary payload instrumentation. The extreme southern extent of the HIPPO transects provides a unique opportunity to examine cloud conditions over the SO, and in this paper we examine high SLW content, evidence of SWRP and large supercooled droplets in different seasons and meteorological conditions.

2. HIPPO missions over the Southern Ocean

Each of the five HIPPO missions included a segment over the Southern Ocean. In four of the flights, the SO segment was a return flight from Christchurch, New Zealand to a maximum southerly latitude of 67° S, but in HIPPO-4 (June 2011) the segment was from Christchurch to Hobart, Australia, with a southerly extent of 58° S. As for the other segments of the missions, these flights were characterized by repeated climbs and descents between low altitude (about 300 m; usually below cloud base) and about 8000 m to establish trace gas and aerosol profiles.

We selected two of the flights for analysis of cloud microphysical conditions based on incidence of appreciable SLW. Of these flights two profiles were chosen for detailed analysis. Research flight 6 during HIPPO-2 (henceforth RF2.06) on 12 November 2009 was conducted in the pre-frontal region of a small but relatively intense mid-latitude cold-core cyclone. Figure 1 shows the flight track plotted over Moderate Resolution Imaging Spectroradiometer (MODIS; on board the NASA A-Train Aqua satellite) cloud top temperature (CTT) retrievals [*Platnick et al.*, 2003]. Near-surface conditions south of 55° S were very calm for the SO with wind speeds around $10\,\mathrm{m\,s^{-1}}$ and video footage below cloud confirming quiet seas. Widespread stratus/stratocumulus fields were present ahead of the frontal band, and the HIAPER penetrated these clouds four times between 2338 and 0140. MODIS CTTs were about -13° C.

During HIPPO-3, research flight 6 (RF3.06) was conducted on 6 April 2010 along the 170° E meridian through a post-frontal airmass. Cold air advection is apparent in the heterogeneous cumulus fields of figure 1, sampled by the aircraft at around 0058 UTC, and further to the south a precipitating stratocumulus deck was sampled at about 0134 and again at 0222. The cloud microphysics instruments on the aircraft varied from one mission to another, but included:

1. Droplet Measurement Technologies (DMT) Ultra High Sensitivity Aerosol Spectrometer (UHSAS), measuring aerosols in the diameter range 0.06 to 1.0 μm (RF 3.06 only),
2. DMT forward-scattering Cloud Droplet Probe (CDP), providing droplet size distribution (DSD) for cloud particle diameter in the range 2 to 50 μm (malfunctioned during RF2.06, and only used for mean particle size in RF3.06),
3. PMS 2D Cloud Imaging Probe (2DC), providing particle images and DSD for particles in the range 62.5 to 1600 μm,
4. King "hot-wire" probe [*King et al.*, 1978] measuring cloud liquid water content (LWC), and
5. A Rosemount icing rate detector (RICE), a qualitative indication of the presence of SLW.

The hot-wire probe was not optimized for the operational speeds of the aircraft and fluctuations in the raw baseline values were evident. These have been zeroed below cloud base for this analysis. Due to inconsistencies between the CDP-derived liquid water content LWC_{CDP} and the hot-wire probe value LWC_{King}, droplet concentration and size distribution from the CDP were disregarded, but the cloud particle radius from the CDP mean droplet diameter ($\overline{D_{CDP}}$) was found to agree well with MODIS retrievals of cloud particle effective radius for cloud top (see small panels of figure 1). Cloud droplet concentrations (Nc; units cm^{-3}) were calculated with:

$$Nc = \frac{6\, LWC_{King}}{\pi \rho_w \, \overline{D_{CDP}}^3} \times 10^{-6}, \quad (1)$$

where ρ_w is the density of liquid water and all parameters (except Nc; hence the factor 10^{-6}) are converted to SI units.

3. Atmospheric profile structure

The thermodynamic profiles for the two southernmost cloud penetrations in RF2.06, at 0111 UTC (63° S) and 0140 UTC (66° S) (figure 2, left panel), shared a number of characteristics. Both profiles show a well-mixed boundary layer below a moderate capping (θ) inversion near 860 hPa (1000 m), with a stratiform cloud layer of 300-400 m depth below this. MODIS retrievals give a CTT of about −15° C and cloud droplet diameters of about 17–20 μm. Hot-wire cloud LWC throughout the profile was close to the value expected for adiabatic ascent. Winds for these profiles were westerly with speeds of 5–10 m s^{-1} and little vertical shear.

The profiles selected from RF3.06, at about 0058 UTC (59° S) and 0222 UTC (66° S) (figure 2, right panel), contrasted in nature. The 0058 profile through an open-celled cumulus field had strong (25 m s^{-1}) south westerly winds with a weak θ inversion coincident with a slight directional wind shift at about 700 hPa/2500 m. The dry sub-cloud layer resulted in a relatively high cloud base (about 800 hPa/1500 m). Temperatures within this cloud ranged from $-16°$ C at cloud base to $-22°$ C near the top. The LWC profile in the top of this cloud is substantially below the expected adiabatic value, due to either condensate removal through precipitation or dry air entrainment at cloud top, or a combination of both processes.

The profile at 0222 was characterized by a stronger inversion at about 815 hPa (1300 m) with stratiform cloud of depth about 500 m (CTT $-18°$ C). The winds were southerly at about 10–12 $\mathrm{m\,s^{-1}}$ near cloud base with a 30° westerly shift through the cloud layer. The LWC profile shows a dip at about 855 hPa before returning to a value consistent with adiabatic condensation, suggesting the traversal of a pocket between cells during the ascent, but heavy icing on the camera housing makes this impossible to verify.

4. Cloud microphysical features

A summary of the cloud microphysical observations for each of the profiles taken in RF2.06 and RF3.06, including those discussed in detail, are shown in table 1 (supplementary material). Some SLW was observed in each of these profiles, evidenced in each case by LWC values $> 0.1\,\mathrm{g\,kg^{-1}}$ at subzero temperatures, RICE signals indicating ice buildup, and visible icing on the time lapse camera housing.

For RF2.06, the cloud depth generally increased to the south, and the maximum LWC (all cloud water was supercooled) values encountered correspondingly increased, consistent with stratiform cloud with adiabatic droplet growth. Drizzle drops (D $> 100\,\mu$m) were observed by the 2DC in three of the five profiles, and two of these profiles also included ice particles. Precipitation observed below cloud was generally at exceptionally low rates with the exception of the first profile.

The cloud layer in RF3.06 was generally deeper with convective cells and correspondingly higher maximum LWC values. Drizzle drops were observed in five out of six profiles where 2DC data was available, and some ice was observed in the same profiles of all but one of these.

Peak LWC values for the 45 second cloud penetration near 0111 UTC during RF2.06 were about 0.2 $\mathrm{gm^{-3}}$. While capable of detecting particles as small as 12.5 μm, the 2DC does not provide an accurate statistical representation of particles smaller than about 50–100 μm due to sizing errors [*Korolev et al.*, 1991]. However, the low number of particles observed (figure 3; left panel, strips 1-4, show all of the 516 particles observed in this profile) suggests that the median diameter of the particles was below the detection threshold for the 2DC. The cloud particle imagery in and just below the cloud layer near 0111 UTC shows that although rare, some precipitation particles were present. Some of these were snowflakes, with dendrite and plate formations particles clearly identifiable, but spherical particles (most likely liquid drops) were also observed, suggesting very low-rate, mixed-phase precipitation. Large crystals are the product of diffusional growth in a saturated environment, and their size and scarcity, combined with the presence of large droplets, suggests that IN were very rare in this environment.

The cloud encountered near 0140 UTC in RF2.06 was thermodynamically similar to the previous profile, with peak LWC of about 0.3 $\mathrm{gm^{-3}}$. In the 60 seconds it took to descend through this cloud layer, some 2150 particles were imaged, with no particles with an area greater than three pixels were observed (see 3; left panel, strips 5-6 for some examples). This indicates that there was virtually no precipitation forming in these clouds. This environment—which was undoubtedly supersaturated with respect to ice, and was still composed predominantly of SLW at the MODIS overpass time 45 minutes later—would have been conducive to rapid crystal growth. The absence of any identifiable ice and the persistence of this cloud strongly suggests that virtually no IN active at temperatures warmer than -15° C were present, although it it impossible to conclude this definitively with the available instrumentation.

Aerosol spectrometer data below the cloudy layer near 0058 UTC in RF3.06 showed a modal sub-cloud dry particle diameter in the range 0.07–0.08 μm, with a total concentration of about 100 cm^{-3} at the lowest flight altitudes, decreasing to about 40 cm^{-3} directly below cloud base, and to about 10 cm^{-3} in the clear air above cloud. Values below 100 cm^{-3} are considered very low by northern hemisphere standards [*O'Dowd et al.*, 2001] but are perhaps to be expected below precipitating clouds in a pristine environment, and the very clean air aloft suggests that the below cloud aerosol was of local origin (i.e. sea salt and biological/organic particles). Mean CPD cloud particle diameter increased from about 20 μm near cloud base to about 30 μm near cloud top. Estimates of Nc from these values and LWC_{King} were 30–50 cm^{-3}; comparable with satellite-derived climatology averages for remote Southern Hemisphere oceans of 40–67 cm^{-3} [*Bennartz*, 2007].

During the ascending profile, large spherical particles were observed in abundance near cloud base (3; right panel, strips 2-3), but not near cloud top (first strip). These are most likely liquid drops (as opposed to frozen) based on high icing rates and the formation of "clear ice" on the time-lapse camera housing. Ice particles were observed very infrequently; the only two clearly identifiable snow flakes are shown in the selected strips. The mean diameter of the particles observed by the 2DC decreases gradually throughout the profile, indicating that the supercooled drizzle was widespread in this cloud rather than existing in an isolated cell. The descending profile, which occurred about eight minutes earlier (some 60 km to the north), was in a different cell altogether, but 2DC observations were similar apart from somewhat higher numbers of snowflakes.

UHSAS aerosol concentration below cloud near 0222 UTC was about 120 cm^{-3}, with above cloud values around 25–40 cm^{-3}. In-cloud Nc was about 80–120 cm^{-3}. Cloud droplets were relatively small, between about 15 μm near cloud base and 20 μm near cloud top, and very few of these were imaged by the 2DC (figure 3; right panel, strips 4-6). In-cloud observations of particles greater than 100 μm diameter were very rare, but "ice drizzle" in the form of very low concentrations of large dendritic crystals was observed below cloud base.

5. Discussion

The HIAPER encountered supercooled liquid stratiform clouds in a variety of conditions and in different seasons over the SO. Although neither the flight plan nor the instrumentation suite was ideally suited for cloud microphysical surveys, the data from these flights provides evidence of the unique cloud conditions.

Consistent with the satellite observations, SLW was observed in appreciable quantities in all of the lowest-level cloud in both of the flights presented in this paper, as well as in other flights where cloud was encountered at subzero temperatures. Geometrically thick low-level clouds are the most common and most energetically important clouds over the SO [*Mace* 2010, *Haynes et al.* 2011], a description which also characterizes the clouds observed in this study. The representation of the coverage, phase and lifetime of these clouds is crucial to accurately simulating the radiative budget and thus the climate of the SO.

Rangno and Hobbs [2001] identified two categories of "moderately" supercooled stratiform clouds (cloud tops $-10°$ to $-20°$ C) in the Arctic: non- or lightly-precipitating (snow and drizzle) with small droplets (D$<20\,\mu$m) and/or high droplet concentrations, and precipitating (snow) with large droplets (D$<20\,\mu$m) at lower concentrations. We found that the clouds observed in the HIPPO flights do not fit easily into either of these categories. The extremely low concentrations of ice particles and the frequent observation of supercooled drizzle and rain suggests that these clouds should not be treated as "Arctic" in nature. However, the sample size for this study is admittedly very small, and the cloud physics instrumentation neglected, and further field observations are required to better characterize these clouds.

Large supercooled drops occurred in persistent stratiform and convective cloud in both pre-frontal and post-frontal environments, in the months of November and April. *Cober et al.* [1996] observed supercooled drizzle drops during a severe icing event in deep maritime stratiform cloud at temperatures between -8 and $-11°$ C near eastern Canada. Conditions were comparable in this extreme event (one of three in 119 hours of in-flight measurements) to the essentially random selection of SO conditions presented in this study, which serves to highlight the unique nature of SO clouds. *Rosenfeld et al.* [2013]

also found supercooled rain in a variety of cloud conditions, but the underlying similarity in those cases was the pristine nature of the airmass with low concentrations of aerosol and IN. Sub-cloud aerosol concentrations were not measured in RF2.06, but were found to be very low during RF3.06. Derived in-cloud Nc was typical for clouds in a remote maritime air mass.

No IN or "small ice" (i.e. $< 100\,\mu$m) measurements were made in the HIPPO flights, but it is inferred from the extremely low concentrations of ice crystals in non-precipitating low-level clouds that IN concentrations effective at $-15°$ to $-20°$ C were very low. While we acknowledge that without more sophisticated instrumentation it is not possible to rule out the existence of small ice particles in these clouds, we consider it unlikely that they would be present in significant concentrations, as they would rapidly grow into large, clearly identifiable ice crystals. In the heavily precipitating clouds where snow was abundant, it is likely that secondary ice processes played an important role.

The hypothesis that supercooled water exists frequently as thin layers over glaciated cloud [*Rauber and Tokay*, 1991] has gained some traction in the cloud remote sensing community, with merged radar/lidar/spectroradiometer satellite products seemingly confirming this structure over the SO [*Huang et al.*, 2012]. However, those authors note some limitations, in particular because of the deficiency in phase attribution of satellite cloud radar retrievals in the temperature range $0°$ to $-20°$ C, and the high attenuation of the lidar signal in liquid clouds. On the other hand, the profiles examined in this paper show quite a different picture of low-level SO clouds: predominantly liquid phase with a mixture of solid and liquid precipitation. The satellite radar phase-retrieval algorithm response to the high-reflectivity (i.e. large) supercooled liquid droplets is most likely to identify ice in SO clouds [*Huang et al.*, 2012], and without a satellite lidar depolarization signal to contradict this, any merged product would be flawed.

Acknowledgments. This research was funded by ARC linkage grant LP120100115 and relies on datasets produced for the HIPPO deployments, and made available to the community by the National Center for Atmospheric Research (NCAR) Earth Observing Laboratory. NCAR is sponsored by the National Science Foundation. This paper has greatly benefited from the insightful comments of Alain Protat and an anonymous reviewer.

References

Bennartz, R. (2007), Global assessment of marine boundary layer cloud droplet number concentration from satellite, *J. Geophys. Res.: Atmos.*, *112*.

Bigg, E. (1973), Ice Nucleus Concentrations in Remote Areas, *J. Atmos. Sci.*, *30*, 1153–1157.

Burrows, S., C. Hoose, U. Pöschl, and M. Lawrence (2013), Ice nuclei in marine air: biogenic particles or dust?, *Atmos. Chem. Phys*, *13*, 245–267.

Cober, S. G., J. W. Strapp, and G. A. Isaac (1996), An example of supercooled drizzle drops formed through a collision-coalescence process, *J. App. Meteorol.*, *35*(12), 2250–2260.

Delanoë, J., and R. J. Hogan (2010), Combined CloudSat-CALIPSO-MODIS retrievals of the properties of ice clouds, *J. Geophys. Res.*, *115*.

DeMott, P. J., A. J. Prenni, and coauthors (2010), Predicting global atmospheric ice nuclei distributions and their impacts on climate, *Proceedings of the National Academy of Sciences*, *107*(25), 11,217–11,222.

Greenwald, T., G. Stephens, S. Christopher, and T. Vonder Haar (1995), Observations of the global characteristics and regional radiative effects of marine cloud liquid water, *J. Clim.*, *8*(12), 2928–2946.

Haynes, J. M., C. Jakob, W. B. Rossow, G. Tselioudis, and J. Brown (2011), Major Characteristics of Southern Ocean Cloud Regimes and Their Effects on the Energy Budget, *J. Clim.*, *24*, 5061–5080.

Hobbs, P. V., and A. L. Rangno (1998), Microstructures of low and middle-level clouds over the Beaufort Sea, *Q. J. R. Meteorol. Soc.*, *124*(550), 2035–2071.

Hu, Y., S. Rodier, and coauthors (2010), Occurrence, liquid water content, and fraction of supercooled water clouds from combined CALIOP/IIR/MODIS measurements, *J. Geophys. Res.*, *115*, D00H34.

Huang, Y., S. T. Siems, M. J. Manton, A. Protat, and J. Delanoë (2012), A study on the low-altitude clouds over the Southern Ocean using the DARDAR-MASK, *J. Geophys. Res.: Atmos.*, *117*, D18204.

Ikeda, K., R. M. Rasmussen, W. D. Hall, and G. Thompson (2007), Observations of freezing drizzle in extratropical cyclonic storms during IMPROVE-2, *J. Atmos. Sci.*, *64*(9), 3016–3043.

King, W. D., D. A. Parkin, and R. J. Handsworth (1978), A hot-wire liquid water device having fully calculable response characteristics, *J. App. Meteorol.*, *17*, 1809–1813.

Korolev, A., S. Kuznetsov, Y. Makarov, and V. Novikov (1991), Evaluation of measurements of particle size and sample area from optical array probes, *J. Atmos. Ocea. Tech.*, *8*(4), 514–522.

Korolev, A. V., G. A. Isaac, and coauthors (2003), Microphysical characterization of mixed-phase clouds, *Q. J. R. Meteorol. Soc.*, *129*(587), 39–65.

Mace, G. G. (2010), Cloud properties and radiative forcing over the maritime storm tracks of the Southern Ocean and North Atlantic derived from A-Train, *J. Geophys. Res.: Atmos.*, *115*.

Morrison, A. E., S. T. Siems, and M. J. Manton (2011), A Three-Year Climatology of Cloud-Top Phase over the Southern Ocean and North Pacific, *J. Clim.*, *24*, 2405–2418.

O'Dowd, C. D., E. Becker, and M. Kulmala (2001), Mid-latitude north-atlantic aerosol characteristics in clean and polluted air, *Atmos. Res.*, *58*(3), 167–185.

Platnick, S., M. D. King, and coauthors (2003), The MODIS cloud products: algorithms and examples from terra, *IEEE Trans. Geosci. Electron*, *41*, 459–473.

Politovich, M. K. (1989), Aircraft Icing Caused by Large Supercooled Droplets., *J. App. Meteorol.*, *28*, 856–868.

Rangno, A. L., and P. V. Hobbs (2001), Ice particles in stratiform clouds in the Arctic and possible mechanisms for the production of high ice concentrations, *J. Geophys. Res.: Atmos.*, *106*, 15,065–15,075.

Rasmussen, R. M., I. Geresdi, G. Thompson, K. Manning, and E. Karplus (2002), Freezing drizzle formation in stably stratified layer clouds: The role of radiative cooling of cloud droplets, cloud condensation nuclei, and ice initiation, *J. Atmos. Sci.*, *59*(4), 837–860.

Rauber, R., and A. Tokay (1991), An explanation for the existence of supercooled water at the top of cold clouds, *J. Atmos. Sci.*, *48*(8), 1005–1023.

Rogers, D. C., P. J. DeMott, S. M. Kreidenweis, and Y. Chen (1998), Measurements of ice nucleating aerosols during SUCCESS, *Geophys. Res. Lett.*, *25*(9), 1383–1386.

Rosenfeld, D., R. Chemke, and coauthors (2013), The common occurrence of highly supercooled drizzle and rain near the coastal regions of the Western United States, *J. Geophys. Res.: Atmos.*

Stephens, G., D. Vane, and coauthors (2002), The CloudSat mission and the A-Train, *Bull. Am. Meteorol. Soc.*, *83*(12), 1771–1790.

Trenberth, K. E., and J. T. Fasullo (2010), Simulation of Present-Day and Twenty-First-Century Energy Budgets of the Southern Oceans, *J. Clim.*, *23*, 440.

Wofsy, S. C., and HIPPO Science Team (2011), HIAPER Pole-to-Pole Observations (HIPPO): Global distributions and emission sources for CH4, N2O, Black Carbon, and other trace species inferred from five aircraft missions, *AGU Fall Meeting Abstracts*.

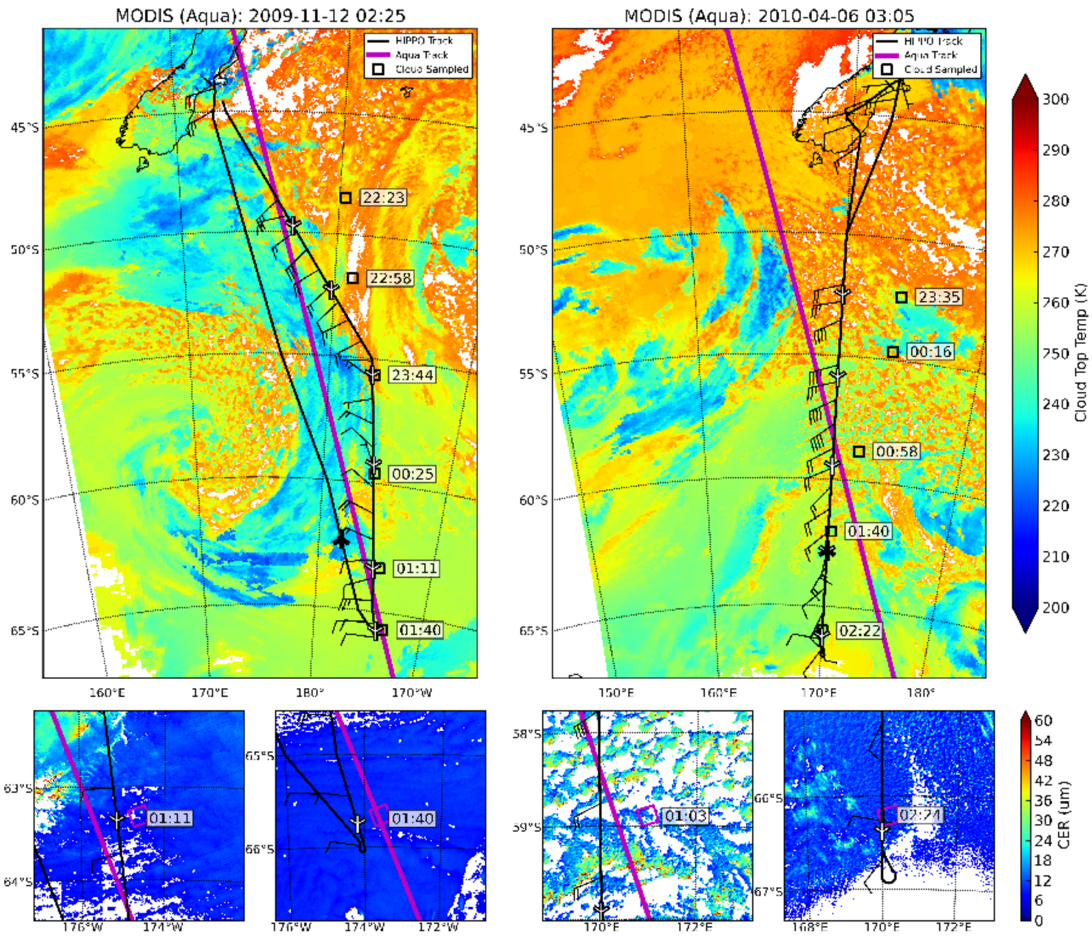

Figure 1. Flight tracks for RF2.06 (left) and RF3.06 (right) overlaid on MODIS cloud top temperature (main panels). Low-level cloud was sampled at the annotated times, with the aircraft position denoted by markers, and the drifted location of the sampled air (based on observed winds) marked by circles. The smaller panels show detail of cloud effective radius near the profiles examined, with the magenta boxes showing a 20 pixel box around the approximate location of the cloud tops observed by the HIAPER.

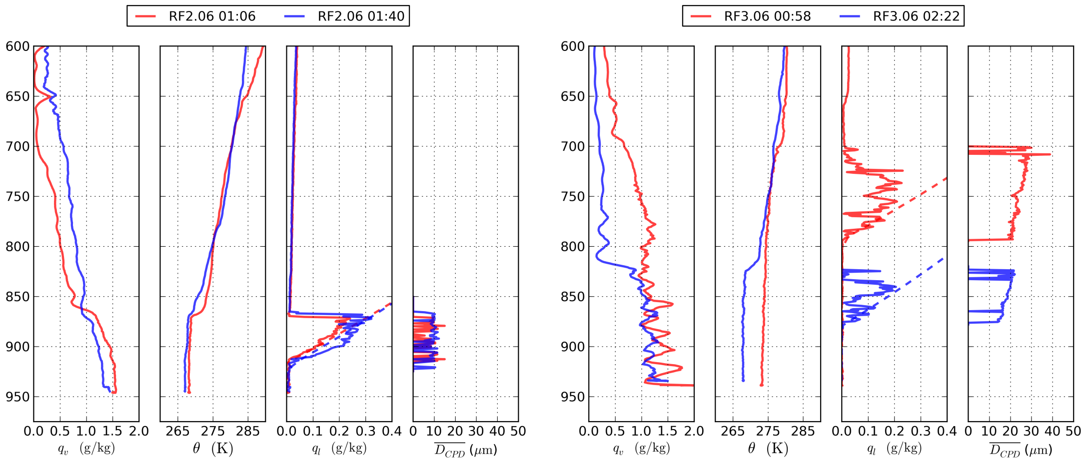

Figure 2. Atmospheric profiles at 0111 UTC (63° S) and 0140 UTC (66° S) during RF2.06 (left), and 0058 UTC (60° S) and 0222 UTC (66° S) during RF3.06 (right), showing water vapor mixing ratio (q_v), potential temperature (θ), liquid water mixing ratio (q_l) and CDP mean droplet diameter ($\overline{D_{CPD}}$; these are not meaningful for RF2.06). The dashed lines represent the adiabatic liquid water mixing ratio initialised from a parcel near cloud base. Fluctuations in the q_v values are due to oscillations in the dew point hygrometers that may last several minutes following descent from cold temperatures.

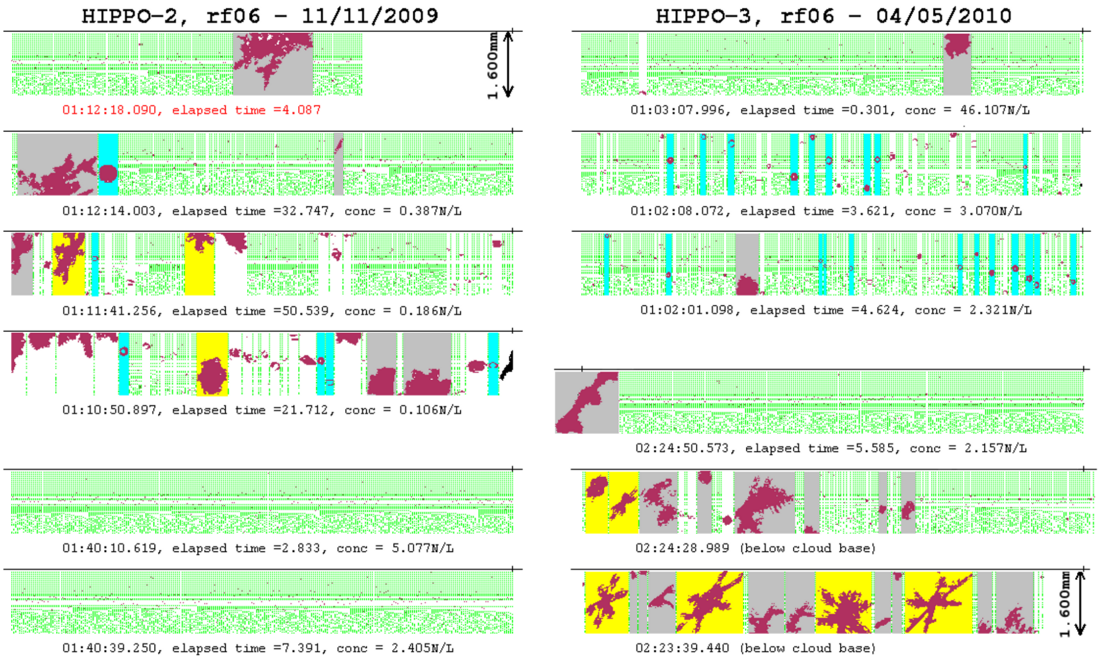

Figure 3. HIPPO 2DC imagery for ascent through cloud layers in RF2.06 near 0111 UTC (left panel, upper four strips), 0140 UTC (left panel, lower two strips), and for cloud layers in RF3.06 near 0058 UTC (right panel, upper three strips), and 0222 UTC (right panel, lower three strips). Strips are arranged in order of altitude for each profile. The time stamps shown are for the last (right-most) particle in the buffer. Coloured backgrounds indicate some particles that have been identified manually; grey indicates an irregular or indeterminate snowflake, yellow are plates and dendritic flakes, while blue background indicates spherical particles.

Table 1. Summary of conditions in (upper section) and below (lower section) low level cloud in RF2.06. Where conditions were similar on ascent and descent profiles, only one is shown, and those profiles discussed in detail in text are marked †. The 2DC ice/liquid particle concentrations are approximate, as there is some ambiguity in the detection of small, round particles. Here, precip. stands for precipitation, dend. stands for dendrite ice crystals, and aggr. stands for aggregate ice crystals.

	RF2.06					RF3.06						
	2223/49 S	2344/55 S	0025/59 S	0111/63 S	0140/66 S	2335/52 S	0016/55 S	0058/59 S	0058/59 S	0140/62 S	0140/62 S	0222/66 S
	ascent	ascent	ascent	ascent†	descent†	ascent	descent	descent	ascent†	descent	ascent	ascent†
Cloud top T (°C)	−11	−15	−15	−15	−16	−11	−13	−18	−22	−18	−17	−18
Cloud depth (m)	250	200	225	350	400	225	500	300	900	600	500	500
LWC_{max} ($g\,m^{-3}$)	0.20	0.17	0.11	0.27	0.37	0.11	0.21	0.45	0.22	0.47	0.47	0.25
Cloud $\overline{D_{CDP}}$ (μm)	–	–	–	–	–	25	20	27	23	29	25	20
2DC Ice (L^{-1})	nil	< 0.01	< 0.01	< 0.01	nil	0.03	0.3	0.4	0.13	–	< 0.01	< 0.01
2DC Lge. drops (L^{-1})	1.4	0.1	nil	0.02	nil	< 0.01	1.0	0.3	0.3	–	1.1	< 0.01
Liquid precip.	rain	drizzle	nil	trace drizzle	nil	trace drizzle	rain	drizzle	drizzle	–	rain	nil
Frozen precip.	nil	dend.	dend.	trace	nil	nil	dend./aggr.	dend./aggr.	trace aggr.	–	trace aggr.	trace dend.
Comments	a	b	c	–	–	d	e	f	–	g	–	–

[a] Ambient temperature below cloud reached about 3°C so mechanism for droplet production (melting snow vs. warm rain) is ambiguous. All cloud water was supercooled.

[b] No cloud sampled in this profile.

[c] Drizzle and large dendrite flakes (D > 3 mm) were co-located in low concentrations during ascent to cloud base.

[d] Large dendrite flakes (D > 3 mm) below cloud base.

[e] Multiple layered cloud, with precipitation falling from upper layer into lower. Large, pristine crystals observed in cloud.

[f] Very heavy snow below cloud base.

[g] 2DC data contaminated due to extreme icing upon entry of cloud layer.